Estimation of Anatomical Connectivity by Anisotropic Front Propagation and Diffusion Tensor Imaging

Marcel Jackowski[1], Chiu Yen Kao[3], and Lawrence Staib[2]

[1] Yale School of Medicine, Dept. of Diagnostic Radiology, New Haven CT 06520
[2] Yale School of Medicine, Dept. of Diagnostic Radiology and Biomedical
Engineering, New Haven CT 06520
[3] University of California Los Angeles, Dept. of Mathematics, Los Angeles CA 90095

Abstract. Diffusion Tensor Magnetic Resonance Imaging (DT-MRI) allows one to capture the restricted diffusion of water molecules in fibrous tissues which can be used to infer their structural organization. In this paper, we propose a novel wavefront propagation method for estimating the connectivity in the white matter of the brain using DT-MRI. First, an anisotropic version of the static Hamilton-Jacobi equation is solved by a sweeping method in order to obtain accurate front arrival times and determine connectivity. Our wavefront then propagates using the diffusion tensor rather than its principal eigenvector, which is prone to misclassification in oblate tensor regions. Furthermore, we show that our method is robust to noise and can estimate connectivity pathways across regions where singularities, such as fiber crossings, are present. Preliminary connectivity results on synthetic data and on a normal human brain are illustrated and discussed.

1 Introduction

While the basic anatomy of white matter tracts in the human brain is generally known from anatomical dissection, much is unknown about its interconnections and its natural variations. Therefore, the characterization and quantitative measurement of its connections is of fundamental importance in understanding brain function. Diffusion Tensor Magnetic Resonance Imaging (DT-MRI) has emerged as a noninvasive imaging modality capable of providing this information in vivo, enabling the detailed study of white matter structure in the human brain.

Brain white matter, because of the long and fibrous nature of axons, exhibits higher restriction to water diffusion across the fibers than along them. This directional variation is measured in diffusivity rates and can be captured by diffusion-weighted MRI. By acquiring diffusion-weighted data in at least six non-collinear directions, it is possible to estimate a 3x3 symmetric matrix (i.e. diffusion tensor) which characterizes diffusion in anisotropic systems [2]. After tensor diagonalization, the eigenvector corresponding to the largest eigenvalue is considered to point along the direction of a fiber bundle.

Numerous connectivity studies relying on the straightforward integration of the principal tensor eigenvector have been described in the literature [4, 3, 9, 8]. Several problems, however, affect their reliability. First, the diffusion images are subject to acquisition noise which can impede the ability to track fibers. Also, while it is true that the principal eigenvector provides an estimate of the microscopic fiber direction, because of partial voluming, signal contributions from multiple tissues can affect individual voxel measurements [1], resulting in a variation in the distribution of fiber directions. This problem becomes more severe when fiber tracts cross, branch or merge.

To account for these variations, level set methods [11] have been employed [12, 10, 7]. These techniques model the evolution of an advancing front through the white matter tracts by following the local directionality provided by the diffusion tensor field. Such methods have been shown to be more robust to noise and singularities than classical streamlining methods. A tractography technique based on Tsitsiklis' fast marching method (FMM) was used by Parker *et al.* [12]. A front was evolved with a speed proportional to the colinearity between the front normal and the principal tensor eigenvector. A discrete approximation of front direction had to be used to drive the evolution through the eigenvector field, since the original FMM cannot handle propagation in oriented domains.

O'Donnell *et al.* [10] posed the connectivity problem in a Riemannian framework where the space is locally warped based on the three eigenvectors and the connectivity corresponds to the lengths of the underlying geodesic paths. Lenglet *et al.* [7] has similarly considered the white matter connectivity problem as one of finding minimal geodesics in the Riemannian space. Both methods employed a less efficient dynamic formulation for the problem, in which a narrow band was employed to constrain front propagation and reduce computation time.

We also propose a level set method to determine connectivity. Unlike other methods, we solve for the true anisotropic solutions of the static front propagation equation. Our sweeping method correctly computes the arrival times so that pathways can be determined. In addition, by using a static perspective of the level set equation, we avoid the localization and separate extraction of zero-level sets at different time steps of the dynamic formulation. Furthermore, the entire diffusion tensor is used to control propagation, avoiding possible biasing of its principal eigenvector in more isotropic regions. In the following, we first model the white matter connectivity problem as one of anisotropic wavefront evolution. We then proceed to describe our propagation equation and the method to solve it. Finally, we present our results on synthetic and real data and conclude.

2   Anatomical Pathways

White matter connectivity can be viewed as an instance of the minimum-cost path problem in an oriented weighted domain. Essentially, one would like to find a fiber path $P(s) : [0, \infty) \mapsto \mathrm{I\!R}^3$ that minimizes some cumulative travel cost from a starting point A to some destination point B in the white matter.

Because of the directionality of the tensor field, the cost function, represented by τ or its reciprocal speed $F = 1/\tau$, is a function of both position $P(s)$ as well as direction $P'(s)$. Hence it is called anisotropic and the minimum cumulative cost at x is defined as:

$$T(x) = \min_P \int_0^L \tau(P(s), P'(s)) \, ds. \tag{1}$$

where L is pathway length, and the starting and ending points are given by $P(0) = A$ and $P(L) = x$. A solution to (1) also satisfies the wave propagation equation:

$$\|\nabla T\| = \tau(x, \nabla T), \tag{2}$$

which describes a wavefront propagating with speed $1/\tau$ where $T(x)$ is the time of arrival of the front at point x. This equation typically arises in problems where a preferred direction of travel exists, such as propagating a front through a vector field. In continuous space, solutions to (2) are given by the Hamilton-Jacobi (HJ) equations. A classical solution to (2) may not exist, and therefore the viscosity solution is commonly sought. Numerical approximations of the viscosity solution can be found in [6, 5, 13].

Once the evolution equation (2) is solved for all points in the domain, one can use the obtained arrival times and find a solution for (1). The minimum-cost path between point A and an arbitrary point B in the white matter then becomes a solution to:

$$\frac{dX}{dt} = -\nabla T, \tag{3}$$

given $X(0) = B$. This optimal path can be constructed by integrating equation (3) at point B back to the seed point A using standard techniques. Next, we will elaborate on the front evolution equation that will be used to trace connectivity pathways in the white matter.

3 Front Propagation Model

We employ the entire tensor in our propagation model to avoid the possible misclassification of the principal eigenvector in oblate tensor regions, which may lead to wrong assignment of front arrival times. We rather design our wavefront to evolve from a seed point A, $T(A) = 0$, at a speed governed by a function of the diffusivity magnitude in the front normal direction $\boldsymbol{n}$:

$$d(\boldsymbol{n}) = \boldsymbol{n}^T D \, \boldsymbol{n}, \quad \boldsymbol{n} = \nabla T / \|\nabla T\|, \tag{4}$$

where D is the diffusion tensor. The motivation behind equation (4) is to let the speed vary locally according to the tensor profile, descriptive of the underlying tissue structure. In addition, we slow down the front more rapidly when diffusivity $d(\boldsymbol{n})$ decreases. Thus, we can write the propagation equation as follows:

$$\|\nabla T\| \cdot \alpha \cdot \exp(d(\boldsymbol{n})^\gamma) = 1, \tag{5}$$

where γ represents the slowing power based on the diffusivity response and α controls the final propagation speed. Since water diffusion measured in the ventricles and in the gray matter is more random than in the white matter, the resulting tensor profile tends to be spherical with eigenvalues $\lambda_1 \simeq \lambda_2 \simeq \lambda_3$. To prevent the propagation into these areas, we choose α to be a measure of diffusion tensor anisotropy. For that, we employed the well-known FA index [2] and after some experimentation, we chose $\alpha = \mathrm{FA}^2$. Parameter γ was also empirically set and yielded smoother results when $\gamma = 2$ or 3.

Propagation equation (5) belongs to a family of static Hamilton-Jacobi equations described by:

$$\begin{cases} H(x, \nabla T) = V(x), \quad x \in \Omega \\ T(x) = q(x) \end{cases} \tag{6}$$

where Ω is the domain in $\mathbb{R}^3$, $V(x) = 1$, and $q(x)$ is a function prescribing boundary condition values, $T(A) = q(A) = 0$. Therefore, we can rewrite (5) as the following Hamiltonian, after discarding the dependence of x on H:

$$H(p, q, r) = \alpha \sqrt{p^2 + q^2 + r^2} \cdot \exp\left\{ \left(\frac{p^2 d_{11} + q^2 d_{22} + r^2 d_{33} + 2pq d_{12} + 2pr d_{13} + 2qr d_{23}}{p^2 + q^2 + r^2} \right)^\gamma \right\} \tag{7}$$

where $p = \partial T/\partial x$, $q = \partial T/\partial y$, $r = \partial T/\partial z$ and d_{ij} are the tensor elements. While equation (5) can be reformulated as a time-dependent HJ equation and solved by recovering each zero-level set, it is more convenient and less computationally expensive to model it as a static problem and determine arrival times instead. In the following section, we will describe an iterative method that solves our static HJ equation (7) so that a viscosity solution can be obtained.

4   Front Propagation Method

Hamiltonians such as (7) cannot be correctly solved by isotropic propagation methods, such as the FMM. However, carefully crafted methods have been devised [6, 5, 13] to construct accurate solutions for anisotropic equations. We use a Lax-Friedrichs (LF) discretization of our Hamiltonian and employ a nonlinear Gauss-Seidel updating scheme [5] to solve the propagation equation. With the LF discretization, a solution at each grid point can be easily obtained in terms of its neighbors. Also, no minimization is required when updating an arrival time, and thus it is very easy to implement.

The Lax-Friedrichs Hamiltonian of equation (7) is defined as:

$$H^{LF} = H\left(\frac{p^+ + p^-}{2}, \frac{q^+ + q^-}{2}, \frac{r^+ + r^-}{2} \right) - \frac{\sigma_x}{2}(p^+ - p^-) - \frac{\sigma_y}{2}(q^+ - q^-) - \frac{\sigma_z}{2}(r^+ - r^-), \tag{8}$$

where $p^\pm$, $q^\pm$ and $r^\pm$ are the forward and backward difference approximations for ∇T, and σ_n is the artificial viscosity which depends on the partial derivative of H with respect to p, q and r.

In order to get a numerical approximation for (7), we solve for $H^{LF} = 1$ by sweeping the domain in the alternating directions $\pm x$, $\pm y$ and $\pm z$. Values from

the previous sweeping step are used to make the approximation decreasing so that it updates an arrival time only if $T_{i,j,k}^{m+1} < T_{i,j,k}^m$. Because the LF method yields a solution utilizing all 6-connected neighbors, values for points outside the boundary of the domain are extrapolated to guarantee the outflow of the solution at the boundary. Sweeping is stopped when the convergence criterion $\|T_{i,j,k}^{m+1} - T_{i,j,k}^m\| \leq \epsilon$ is met. Details on the algorithm, accuracy and convergence of LF sweeping (LFS) scheme can be found in Kao *et al.* [5].
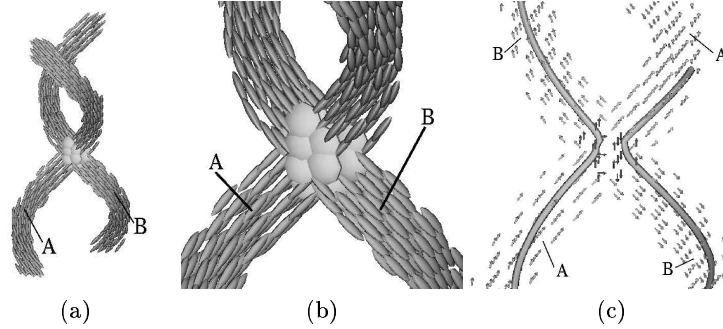

Fig. 1. (a) Synthetic tensor dataset containing two fiber bundles with main diffusivities $\{9, 2, 1\}$ mm^2/s. (b) Close-up look of the fiber-crossing location and resulting oblate tensors. (c). Result from streamline integration across the fiber-crossing region.

5   Results

Figure 1a shows our synthetic model consisting of two fiber bundles A, B oriented along helical paths which cross each other at their middle section (Fig. 1a). The background was filled with nearly isotropic tensors ($\{4, 3, 2\}$ mm^2/s, not shown). Fig. 1b depicts a close-up view of the fiber-crossing region, where oblate tensors resulting from the crossing are found. Figure 1c depicts a failed attempt in reconstructing pathways from bundles A and B using the streamlining technique. The oblate tensors in the fiber crossing region erroneously advected both pathways away from their true trajectories.

Using our method, we reconstructed the same pathways to demonstrate that it can handle the fiber crossing without deviating the fiber trajectories. First, diffusion-weighted images were created from our model, and increasing levels of Gaussian noise ($\sigma^2 = 0.05$, 0.15 and 0.2) were added to them. The resulting tensor images are shown in Fig. 2a-c. Then, a seed point A_1 was fixed at the bottom of bundle A (Fig. 2a) and our wavefront ($\gamma=2$) was propagated using the LFS method on the tensor images. Points A_2, B_1 and B_2 were fixed at the extreme ends of each bundle (Fig. 2a) and corresponding pathways A_2A_1, B_1A_1 and B_2A_1 were traced on ∇T images using a Runge-Kutta 4th-order integration.

Figures 2d, 2e, 2f illustrate the obtained connectivity pathways embedded in the arrival time images and corresponding arrival isocurves (up to time 100). Darker areas in the maps reveal earlier arrivals. The LFS method converged to a solution ($\epsilon = 10^{-3}$), after 30 iterations for results in Figs. 2d, 2e, and after 40 iterations in Fig. 2f. As can be seen, the singularity region did not prevent pathways connecting different branches or same branch (A_2A_1) from being recovered. To assess the variability of the extracted paths, we propagated the same front in the diffusion tensor image without added noise and then computed the mean distance between corresponding pathways. Mean distance for all paths under noise $\sigma^2=0.05$ was 1.06 voxels, for $\sigma^2=0.15$ mean distance was 1.22 voxels and for $\sigma^2=0.20$, it was 1.65 voxels. Therefore the recovered pathways remained very close to their trajectories, in spite of the added noise.
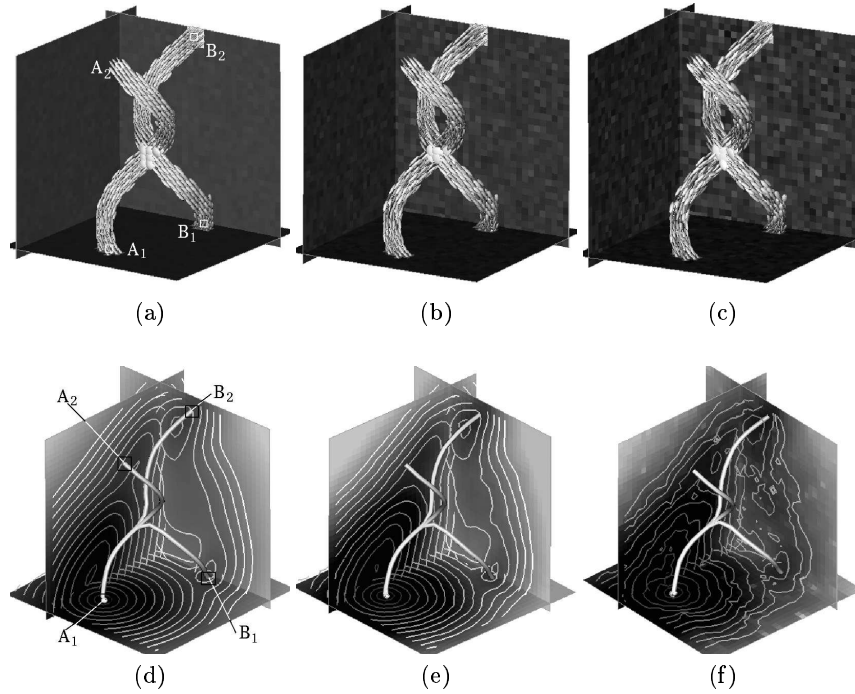

Fig. 2. (a-c) Tensor model with additive Gaussian noise ($\sigma^2 = 0.05$, 0.15 and 0.20). (d-f) Times of arrival and connectivity pathways corresponding to images (a-c), respectively.

A diffusion-weighted image was acquired using a Siemens 3T Trio scanner with a standard coil. A single-shot EPI image of matrix size 128x128x40, resolution 2x2x3 mm^3, b-factors 0 and 1000 s/mm^{-2}, and 32 gradient directions uniformly sampled on a sphere was obtained. The diffusion tensor was calculated from a total of 12 averages to maximize signal to noise ratio. In this dataset, we

fixed the seed point in the splenium of the corpus callosum (Fig. 3a). We then propagated our wavefront throughout the image using the LFS method. A total of 25 iterations were needed for convergence. Figure 3a depicts the resulting arrival time level sets between 0 and 500. In order to trace connectivity pathways to the splenium, we first obtained a rough boundary of the white matter according to the following procedure. The FA image was thresholded at 0.18, in order to obtain all points belonging to the white matter. Next, by using a morphological operator, we determined the inner boundary of the thresholded region. All pathways between points on this boundary and the point in the splenium were traced using the map of arrival times. Fig. 3b shows the resulting 20,817 pathways, colored by the FA value at each point, where brighter points represent higher anisotropy. In Figures 3b and 3c, we can observe the main routes of connection between various brain regions and the splenium. Points leaving the genu of the corpus callosum (CC) connect to the splenium via the cingulum (CI) pathways, and points in the superior frontal lobe connect via the superior longitudinal fasciculi (SL) consistent with known anatomy.

Not all connections shown in figures 3b and 3c represent true anatomical pathways. A metric to rate their anatomical likelihood such as the co-linearity between pathway tangent and principal eigenvector as described by Parker *et al.* [12] will be investigated. In future work, we plan to propagate our wavefront from all points belonging to the white matter boundary and then trace all possible pathways back to corresponding seed points. By using geometric properties such as pathway length and tangent, as well as measures derived from diffusion images, we plan to design an automated system for brain fiber recovery.
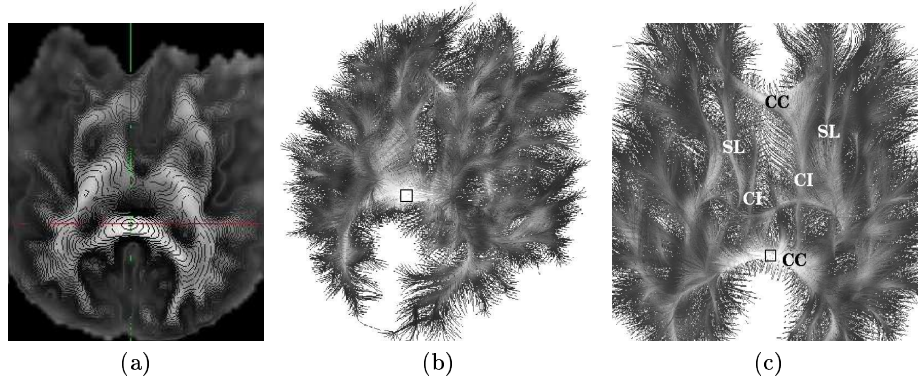

(a) (b) (c)

Fig. 3. (a) Level sets depicting arrival times between 0 and 500, after propagation using the LFS method. (b) 20,817 different pathways connecting white matter boundary to the splenium of the corpus callosum were extracted. (c) Close-up view of the main pathways connecting to the splenium.

6 Conclusions

An anisotropic front propagation method was described for determining connectivity pathways in the white matter. It successfully recovered pathways embedded in different levels of noise and was able to extract paths of connection across areas of singularities in the diffusion tensor, unlike streamlining techniques. The use of the static perspective of the level set equation allowed us to pose the problem so that front arrival times could be easily computed. Moreover, our formulation used the entire tensor for propagation, avoiding the possible biasing in the eigenvector classification. Finally, results on a real diffusion tensor dataset were presented where major fiber bundles were identified and were consistent with known anatomy.

References

1. A. L. Alexander, K. M. Hasan, M. Lazar, J. S. Tsuruda, and D. L. Parker. Analysis of partial volume effects in diffusion-tensor MRI. *Mag. Res. Medicine*, 45(5):770–780, May 2001.
2. P. J. Basser and C. Pierpaoli. Microstructural and physiological features of tissues elucidated by quantitative-diffusion-tensor MRI. *J. Mag. Res., Series B*, 111(3):209–219, Jun 1996.
3. P.J. Basser, S. Pajevic, C. PierPaoli, J. Duda, and A. Aldroubi. In-vivo fiber tractography using DT-MRI data. *Mag. Res. Medicine*, 44:625–632, 2000.
4. D. K. Jones, A. Simmons, S. C. Williams, and M. A. Horsfield. Noninvasive assessment of axonal fiber connectivity in the human brain via diffusion tensor MRI. *Mag. Res. Medicine*, 42:37–41, 1999.
5. C. Kao, S. Osher, and J. Qian. Lax-Friedrichs Sweeping scheme for static Hamilton-Jacobi equations. *Journal of Computational Physics*, in press, 2003.
6. C. Kao, S. Osher, and Y. Tsai. Fast Sweeping Methods for static Hamilton-Jacobi equations. Technical report, University of California Los Angeles, 2002. ftp://ftp.math.ucla.edu/pub/camreport/cam02-66.pdf.
7. C. Lenglet, R. Deriche, and O. Faugeras. Diffusion tensor magnetic resonance imaging: Brain connectivity mapping. Research Report 4983, INRIA, 2003.
8. N. F. Lori, E. Akbudak, J. S. Shimony, T. S. Cull, A. Z. Snyder, R. K. Guillory, and T. E. Conturo. Diffusion tensor fiber tracking of human brain connectivity: aquisition methods, reliability analysis and biological results. *NMR in Biomedicine*, 15(7-8):494–515, 2002.
9. S. Mori and P. C. M. van Zijl. Fiber tracking: principles and strategies - a technical review. *NMR in Biomedicine*, 15(7-8):468–480, 2002.
10. L. O'Donnell, S. Haker, and C.-F. Westin. New approaches to estimation of white matter connectivity in diffusion tensor MRI: Elliptic PDEs and geodesics in a tensor-warped space. *Proc. MICCAI*, pages 459–466, 2002.
11. S. Osher and R. Fedkiw. *Level Set Methods and Dynamic Implicit Surfaces*. Springer-Verlag New York Inc, 1st edition, 2003.
12. G. J. M. Parker, C. A. M. Wheeler-Kingshott, and G. J. Barker. Estimating distributed anatomical connectivity using fast marching methods and diffusion tensor imaging. *IEEE Trans. Med. Imaging*, 21(5):505–512, 2002.
13. J. A. Sethian and A. Vladimirsky. Ordered Upwind Methods for static Hamilton-Jacobi equations. *PNAS*, 98(20), September 2001.